Hybrid magnetoresistance in the proximity of a ferromagnet

Y. M. Lu, J. W. Cai, S. Y. Huang, D. Qu, B. F. Miao, and C. L. Chien

Phys. Rev. B **87**, 220409 — Published 28 June 2013

DOI: 10.1103/PhysRevB.87.220409

Submitted Nov. 12, 2012

Hybrid Magnetoresistance in the Proximity of a Ferromagnet

Y. M. Lu,[1] J. W. Cai,[1,*] S. Y. Huang,[2] D. Qu,[2] B. F. Miao,[2,3] and C. L. Chien[2,†]

[1] Beijing National Laboratory for Condensed Matter Physics, Institute of Physics, Chinese Academy of Sciences, Beijing 100190, China

[2] Department of Physics and Astronomy, Johns Hopkins University, Baltimore MD 21218 USA

[3] National Laboratory of Solid State Microstructures and Department of Physics, Nanjing University, Nanjing 210093, China

Abstract

We report a new magnetoresistance (MR) effect observed in nominally non-magnetic metal (Pt) thin film in contact with either a ferromagnetic insulator or a ferromagnetic metal. The resistivities with in-plane magnetic field parallel ($\rho_{\parallel}$) and transverse (ρ_{T}) to current, and perpendicular field ($\rho_{\perp}$) show the behavior of $\rho_{\perp} \approx \rho_{\parallel} > \rho_{T}$, distinctly different from all other known MR effects, including anisotropic MR with $\rho_{\parallel} > \rho_{T} \approx \rho_{\perp}$. We termed the new MR hybrid MR, which appears in a metal in close proximity with a ferromagnet either insulating or metallic, and is associated with the induced magnetic moments at the interface.

PACS numbers: 72.25.Mk, 75.70.-i, 75.47.-m, 72.25.Ba

Phenomena of pure spin current have recently attracted a great deal of attention [1-10]. A pure spin current can be generated only by a few methods, which include non-local spin injection in lateral structures [1,2], spin-pumping [3,4], spin Hall effect (SHE) [5,6], and spin Seebeck effect (SSE) [7-11]. For example, the SHE can convert a charge current in a non-magnetic metal with strong spin-orbit coupling (SOC) into a pure spin current in the transverse direction. Once generated, a pure spin current cannot be detected by the usual electrical means except through a pure spin current detector. The most widely used method is the inverse spin Hall effect (ISHE), which converts the pure spin current into a charge current resulting in charge accumulation in the transverse direction. Platinum (Pt) metal in contact with a ferromagnet, either metallic or insulating, has been most often employed for this essential role. The recent observation of magnetic proximity effects (MPE) in Pt/YIG, where YIG = yittrium iron garnet =$Y_3Fe_5O_{12}$, questions the suitability of Pt as a spin current detector [12].

Interestingly, Pt/YIG also exhibits a new type of MR with unique characteristics that are very different from those of other known MR phenomena. Very recently Nakayama *et al.* [13], have proposed a theory of spin Hall magnetoresistance (SMR) in a non-magnetic metal with strong SOC in contact with a ferromagnetic insulator to account for the new MR in Pt/YIG [13-16]. It involves a conversion of charge/spin current by the SHE and the ISHE within Pt in contact with YIG. The report of this new MR so far has been limited to ferromagnetic insulator, YIG. However, we show in this work that the new MR, in addition to Pt/YIG, has also been realized in Pt/Py, where Py = permalloy = $Ni_{80}Fe_{20}$ is a ferromagnetic metal. We term the new MR hybrid MR, which occurs more generally in systems involving a metal layer in the proximity of a ferromagnet, either a

metal or an insulator. Among the systems investigated, it appears that the occurrence of the hybrid MR coincides with the evidence of induced moments due to MPE.

The thickness dependence of electrical resistivity ρ and MR of a metallic layer often reveals the underlying mechanisms. The value of ρ is independent of the layer thickness t except at small thicknesses when t is comparable to, or less than, the carrier mean free path l [17,18]. As a result of the emergence of increasing surface scattering, ρ increases sharply with decreasing t. This behavior is illustrated by the results of Pt thin films as shown in Fig. 1(a). Under a magnetic field $\boldsymbol{H}$, the MR of Pt, as in most other non-magnetic metals, is negligibly small. In ferromagnetic (FM) metals, however, there is anisotropic MR (AMR), which depends on the angle ϕ between the direction of the magnetization $\boldsymbol{M}$ as aligned by $\boldsymbol{H}$ in the film plane and that of the electrical current I,

$$\rho(\phi) = \rho_{\perp} + (\rho_{\parallel} - \rho_{\perp}) \cos^2\phi \qquad (1)$$

where $\rho_{\parallel}$ and $\rho_{\perp}$ are respectively the longitudinal ($\boldsymbol{M} \parallel I$) and the transverse resistivity ($\boldsymbol{M} \perp I$) [19,20]. For many FM transition metal alloys, including Py, the AMR exhibits $\Delta\rho = \rho_{\parallel} - \rho_{\perp} > 0$. The magnitude of AMR $\Delta\rho/\rho$ is only a few percent, but highly sensitive to small magnetic fields thus technologically important as field sensors. The AMR value $\Delta\rho/\rho$ is independent of thickness except in very thin FM films where $\Delta\rho/\rho$ decreases sharply, as shown in Fig. 1(b), due to the rapidly rising ρ as mentioned above. The hybrid MR shows very different characteristics.

In this work, we use magnetron sputtering to fabricate metal thin films (Pt, Py, Au, etc.) onto epitaxial and polycrystalline ferromagnetic insulator YIG as well as other

common substrates to reveal the characteristics of the hybrid MR. The epitaxial YIG layer, grown by liquid-phase-epitaxy onto GGG (gadolinium gallium garnet = $Gd_3Ga_5O_{12}$) substrate, has a roughness of 0.3 nm. We have found that if the YIG surface has been altered, the resultant MPE and MR properties can be drastically altered. Thus, all the measurements have been made on samples cut from the same or similar specimen. We use four-probe resistance measurements on patterned Hall-bar thin films, where the film plane is in the *xy*-plane, with the current *I* in the *x*-direction, and the voltage is measured by the two side electrodes as shown in Fig. 1(d). In FM films with in-plane anisotropy, by using a magnetic field ***H*** in the *xy*-plane (ϕ_{xy}-scan) to align ***M***, one can measure $\rho_{\|}$, ρ_{Γ}, and obtain the angular dependence as described by Eq. (1). One can also apply a large ***H*** (much larger than the shape anisotropy field of the FM film) in the *xz*-plane (α_{xz}-scan) or the *yz*-plane (θ_{yz}-scan) to access the perpendicular resistivity $\rho_{\perp}$ with ***M*** perpendicular to the film plane along the *z*-axis. Referring to the measuring geometry in Fig. 1(d), $\rho_{\|}$, ρ_{Γ}, and $\rho_{\perp}$ are the resistivities ρ_x, ρ_y, and ρ_z, with ***M*** along the *x, y*, and *z* respectively.

Representative AMR results of Py using the ϕ_{xy}-scan, the α_{xz}-scan, and the θ_{yz}-scan are shown in black, red, and blue respectively in Fig. 2(a) and 2(b). With an in-plane field, the ϕ_{xy}-scan shows the $\cos^2\phi_{xy}$ dependence described in Eq.(1). Under a large field (e.g., 40 kOe) to align ***M*** along ***H***, the α_{xz}-scan also shows the $\cos^2\alpha_{xz}$ dependence. The field dependence of MR will be discussed later. For FM films with in-plane anisotropy, since $\rho_{\Gamma} \approx \rho_{\perp}$, the θ_{yz}-scan provides little variation. The slight difference between ρ_{Γ} and

$\rho_\perp$ is due to the geometrical size effects of AMR [21-23]. The α_{xz}-scan, requiring much larger fields but yields the same results as that of the ϕ_{xy}-scan, remains the most useful. The characteristics of AMR of Py are therefore

$$\text{AMR:} \quad \rho_\parallel > \rho_\Gamma, \quad \rho_\Gamma \approx \rho_\perp, \tag{2}$$

and that θ_{yz}-scan ≈ constant, α_{xz}-scan ≈ ϕ_{xy}-scan. The AMR magnitude $\Delta\rho/\rho \approx$ constant except at very small t, where $\Delta\rho/\rho$ decreases towards zero, as shown in Fig. 2(c) and 2(d) for the three separate resistivities. Because SiO_2 and Au are quite inert, both Au/Py(t_{Py})/Au and SiO_2/Py(t_{Py})/SiO_2 show only the AMR.

We next describe the unusual MR results of Pt/YIG. Thin Pt films on a non-magnetic and insulating substrate, such as Pt/Si, show no measurable MR as expected. In contrast, Pt/YIG shows a pronounced MR as recently reported [11,12]. The ϕ_{xy}-scan results of Pt/YIG have the $\cos^2\phi_{xy}$ angular dependence, and $\rho_\parallel > \rho_\Gamma$, same as those of Py as shown in Fig. 3(a). However, the other MR characteristics of Pt/YIG are very different. Most notably, as shown in Fig. 3(a), the θ_{yz}-scan shows the *same* angular dependence with the same amplitude as that of the ϕ_{xy}-scan, whereas the α_{xz}-scan shows *no* variation. These are the hybrid MR behavior of Pt/YIG of

$$\text{Hybrid MR:} \quad \rho_\parallel > \rho_\Gamma, \quad \rho_\parallel \approx \rho_\perp, \tag{3}$$

and that α_{xz}-scan ≈ constant, θ_{yz}-scan ≈ ϕ_{xy}-scan, which are maintained for the samples of *all* thicknesses as shown in Fig. 3(c). It is important to stress the difference between AMR and hybrid MR. In both AMR and the hybrid MR, $\rho_{\parallel} > \rho_{\Gamma}$ and that the ϕ_{xy}-scan shows the $\cos^2\phi_{xy}$ dependence. The key difference is $\rho_{\perp}$, which is $\rho_{\perp} \approx \rho_{\Gamma}$ in AMR but $\rho_{\perp} \approx \rho_{\parallel}$ in the hybrid MR. Consequently, the amplitude in α_{xz}-scan is unique to AMR, whereas that in the θ_{yz}-scan is unique to the hybrid MR. The samples of Pt on a liquid phase epitaxial YIG film grown on GGG substrates give similar results with those on polished polycrystalline YIG substrates. All the angular scans of α_{xz}, θ_{yz}, and ϕ_{xy} show the same (cosine)^2 dependence.

The magnitude $\Delta\rho/\rho$ of the unusual hybrid MR is *not* constant but decreases with increasing t approximately as $1/t$ and approaches zero at large t as shown in Fig. 1(c). Remarkably, at very small t (e.g., 2 nm) $\Delta\rho/\rho$ continues to increase notwithstanding the rapidly rising ρ value, before eventually decreasing. These features indicate that the scattering events that cause the hybrid MR are *at or near* the interface and coupled to YIG. Increasing the Pt layer thickness only dilutes $\Delta\rho$, thus $\Delta\rho/\rho$ decreases with t and becomes vanishing small at larger t. In contrast, both $\Delta\rho$ and ρ in AMR are unchanged at large layer thicknesses because *all* the magnetic moments in the layer contribute to scattering.

The SMR mechanism is based on the continuous conversion between charge and spin current within the Pt layer due to SHE and ISHE [13]. The spin current is absorbed

($\boldsymbol{\sigma}\perp\boldsymbol{M}$) or reflected ($\boldsymbol{\sigma}\parallel\boldsymbol{M}$) at the YIG surface, depending on the magnetization direction due to the spin-transfer torque effects, where $\boldsymbol{\sigma}$ is spin direction along the *y*-axis in Pt and $\boldsymbol{M}$ is the magnetization in YIG. This model is based on the premise that Pt is a non-magnetic metal with strong SOC but with no induced magnetic moment.

However, there are ample evidences of induced Pt moments due to the MPE in Pt/YIG. In addition to MR, other evidences of Pt moments include anomalous Hall effect, anomalous Nernst effect [12], theoretical calculations [24], and most recently from x-ray magnetic circular dichroism (XMCD), which provides a direct confirmation of the Pt moment through the characteristic x-ray of Pt [25]. While some metals (e.g., Pt) are susceptible to acute MPE, others (e.g., Au) show no MPE effects [24]. The theory of spin MR would be also applicable for Au/YIG, a truly non-magnetic metal with strong SOC. Yet, no appreciable MR has been observed in Au/YIG [24]. The nature of the new MR may be revealed in systems beyond Pt/YIG and Au/YIG.

The strong MPE in Pt in contact with FM metals, including Pt/Co [26], Pt/Ni [27], and Pt/Fe [28], has been long standing as confirmed conclusively by XMCD. We show that the hybrid MR that appears in Pt/YIG *also* appears in Pt/Py, for which the MPE and induced Pt moments are well established. We have measured a series of Pt(3 nm)/Py(t_{Py})/Pt(1.5 nm) samples, for which the MR results in the ϕ_{xy}-scan (black), the α_{xz}-scan (red), and the θ_{yz}-scan (blue) can be well described by (cosine)^2 as shown in Fig. 3(b). However, the MR result in each case is the *sum* of the AMR due to Py and the hybrid MR due to the Pt/Py interface. Because AMR and hybrid MR have the same angular dependence in the ϕ_{xy}-scan (black), there is a single $\cos^2\phi_{xy}$ dependence with its amplitude

as the sum of those of AMR and hybrid MR. However, the α_{xz}-scan (red) shows only the AMR of Py (Fig. 2(a)) since the hybrid MR is unchanged (Fig. 3(a)). The AMR amplitudes are shown as the vertical red arrows in Fig. 2(a) and Fig. 3(b). In the θ_{yz}-scan (blue), since AMR is nearly unchanged (Fig. 2(a)), one measures only the hybrid MR contribution, the same as that in Pt/YIG (Fig. 3(a)). The vertical blue arrows in Fig. 3(a) and 3(b) indicate the hybrid MR amplitude. In this manner, the new MR can be unequivocally identified even with the presence of the AMR from Py. Similar behavior has earlier been observed in Pt/Co/Pt sandwiches [29] but without identifying the mechanism. The thickness dependence (Fig. 3(d)) of the MR in Pt(3 nm)/Py(t_{Py})/Pt(1.5 nm) shows mainly AMR at large t_{Py} (e.g., 10 nm) and the hybrid MR emerges at small t_{Py}, (e.g., 2 nm), reflecting respectively the bulk and interfacial nature of the two MR effects. Previously the presence of MPE in Pt in contact with a FM metal such as Co, Ni, and Fe, has been confirmed by XMCD [26-28]. Our results show that the presence (e.g., in Pt/Py/Pt), and the absence (e.g., in Au/Py/Au) of MPE in contact with an FM metal can also be revealed by MR measurements, in addition to XMCD.

The MPE observed in Pt/YIG is not entirely surprising since Pt, in light of the Stoner's criterion, is one of the marginally magnetic elements, on the verge of being FM [30,31]. A more interesting question is whether a FM metal, such as Py, can also acquire MPE. The MR results of Py(4 nm)/YIG in Fig. 4(a) show that in addition to the AMR (indicated by the red arrow) inherent to Py, there is also the hybrid MR (indicated by the blue arrow) as a result of the contact with YIG. The conclusion is further confirmed in the results for different Py thicknesses. Thus MPE, as revealed by the hybrid MR, occurs

in Pt/YIG, Pt/Py, as well as Py/YIG, encompassing metallic as well as insulating ferromagnets with the same MR phenomena, suggests a common mechanism.

We mention the field dependence and temperature effects of MR measurements. For FM films with in-plane anisotropy, only a small magnetic field is needed in the ϕ_{xy}-scan. In the α_{xz}-scan and the θ_{yz}-scan, the shape anisotropy demands a much larger $\boldsymbol{H}$ to align $\boldsymbol{M}$. For example, in the α_{xz}-scan, the Zeeman energy together with shape anisotropy energy of $-\boldsymbol{H}\cdot\boldsymbol{M}$ $-\mu_o M^2\cos\alpha/2$ determine the resultant orientation of $\boldsymbol{M}$. Consequently, one observes an angular dependence of $|\cos\alpha|$ at modest fields (e.g., H = 14 kOe) before evolving to $\cos^2\alpha$ at large fields (e.g., 40 kOe) (Fig. 4(c)). Since at elevated temperatures, the resistance decreases with H due to decreasing spin disorder scattering [19] (Fig. 4(d)) there is a small downward shift of the resistance curves at larger fields measured at 300 K (Fig. 4(b)) but not at 4 K.

All the angular scans of the hybrid MR show the (cosine)^2 dependence. According to the SMR theory, the (cosine)^2 dependence is the subtle result of a vector double cross product [13]. However, we note the (cosine)^2 dependence is a general consequence of anisotropic transport in thin film, whenever the electrical field $\boldsymbol{E}$ is not collinear with the current density $\boldsymbol{j}$ [19,20]. For this reason, the AMR of ferromagnetic thin film shows the (cosine)^2 dependence.

Aside from the common (cosine)^2 dependence, the AMR ($\rho_{\parallel} > \rho_{\Gamma} \approx \rho_{\perp}$) and the hybrid MR ($\rho_{\perp} \approx \rho_{\parallel} > \rho_{\Gamma}$) differ only in the perpendicular resistivity $\rho_{\perp}$. The conventional AMR in FM metals is due to *s-d* scattering, determined by the angle

between the magnetization and current direction. The AMR characteristics of $\rho_{\parallel} > \rho_{T} \approx \rho_{\perp}$ reflects the shape of the *d*-orbital of the FM moments when the magnetic moment $\boldsymbol{\mu}$ is compelled to rotate with $\boldsymbol{H}$ [19,20]. The hybrid MR shows a completely different behavior of $\rho_{\perp} \approx \rho_{\parallel} > \rho_{T}$. In addition to Pt/YIG, the hybrid MR also exists in Py/Pt and Py/YIG, but absent in Au/YIG. The newly proposed SMR theory is intended to be applicable in Pt/YIG, in which the spin/charge current in the non-magnetic Pt layer can be absorbed or reflected off the surface of the FM insulator YIG. However, the evidences of MPE in Pt/YIG complicate the situation. Beside, in the case of Pt/Py, the absorption or reflection of the spin/charge current off the surface of a FM metal would be much different from those of a FM insulator. Yet, the same MR behavior has been observed in Pt/Py. More significantly, the MPE and the induced moments in Pt/Py as well as Pt with other FM metals, have been long standing. From the known results to date in Pt/YIG, Pt/Py, and Pt/YIG, the hybrid MR exists in every case where MPE and induced magnetic moments are well known or strongly suggested.

In summary, the angular dependent MR studies and thickness dependence of the constituent layers allow unambiguous observation of a new type of MR, termed hybrid MR, with characteristics of $\rho_{\parallel} > \rho_{T}$, $\rho_{\parallel} \approx \rho_{\perp}$, which is different from those of other known MR phenomena. We show that the presence of the hybrid MR coincides with the evidence of MPE and induced magnetic moments near the interface with an FM material, either insulating (YIG) or a metallic (Py). The hybrid MR in Pt/YIG, Pt/Py, and Py/YIG shows the same phenomena, thus suggesting a common mechanism. The more generally

observed MR appears to be beyond the scope of the newly proposed SMR theory for Pt/YIG.

Acknowledgments: The work at Chinese Academy of Sciences was supported by MSTC (Grant No. 2009CB929201) and NSFC (Grant Nos. 51171205, 51021061 and 50831002). The work at Johns Hopkins University was supported by US DOE (DE-SC0009390). BFM was supported by the Yeung Center at JHU and the State Key Program for Basic Research of China (Grant No. 2010CB923401).

References:

*jwcai@iphy.ac.cn

†clc@pha.jhu.edu

1. S. O. Valenzuela and M. Tinkham, Nature (London) **442**, 176 (2006).
2. T. Kimura, Y. Otani, T. Sato, S. Takahashi, and S. Maekawa, Phys. Rev. Lett. **98**, 156601 (2007).
3. E. Saitoh, M. Ueda, H. Miyajima, and G. Tatara, Appl. Phys. Lett. **88**, 182509 (2006).
4. K. Ando, Y. Kajiwara, S. Takahashi, S. Maekawa, K. Takemoto, M. Takatsu, and E. Saitoh, Phys. Rev. B **78**, 014413 (2008).
5. J. E. Hirsch, Phys. Rev. Lett. **83**, 1834 (1999).
6. Y. K. Kato, R. C. Myers, A. C. Gossard, and D. D. Awschalom, Science **306**, 1910 (2004).
7. K. Uchida, S. Takahashi, K. Harii, J. Ieda, W. Koshibae, K. Ando, S. Maekawa, and E. Saitoh, Nature (London) **455**, 778 (2008).

8. K. Uchida, J. Xiao, H. Adachi, J. Ohe, S. Takahashi, J. Ieda, T. Ota, Y. Kajiwara, H. Umezawa, H. Kawai, G. E. W. Bauer, S. Maekawa, and E. Saitoh, Nature Mater. **9**, 894 (2010).
9. C. M. Jaworski, J. Yang, S. Mack, D. D. Awschalom, J. P. Heremans, and R. C. Myers, Nature Mater. **9**, 898 (2010).
10. K. Uchida, H. Adachi, T. Ota, H. Nakayama, S. Maekawa, and E. Saitoh, Appl. Phys. Lett. **97**, 172505 (2010).
11. M. Weiler, M. Althammer, F. D. Czeschka, H. Huebl, M. S. Wagner, M. Opel, I. M. Imort, G. Reiss, A. Thomas, R. Gross, and S. T. B. Goennenwein, Phys. Rev. Lett. **108**, 106602 (2012).
12. S. Y. Huang, X. Fan, D. Qu, Y. P. Chen, W. G. Wang, J. Wu, T. Y. Chen, J. Q. Xiao, and C. L. Chien, Phys. Rev. Lett. **109**, 107204 (2012).
13. Nakayama et al., Phys. Rev. Lett. **110**, 206601 (2013).
14. Y.-T. Chen, S. Takahashi, H. Nakayama, M. Althammer, S. T. B. Goennenwein, E. Saitoh, and G. E. W. Bauer, Phys. Rev. B **87**, 144411 (2013)
15. C. Hahn, G. de Loubens, O. Klein, M. Viret, V. V. Naletov, and J. Ben Youssef, Phys. Rev. B **87**, 174417 (2013).
16. N. Vlietstra, J. Shan, V. Castel, B. J. van Wess, and J. Ben Youssef, Phys. Rev. B **87**, 184421 (2013).
17. K. Fuchs, Mathematical Proceedings of the Cambridge Philosophical Society **34**, 100108 (1938).
18. E. H. Sondheimer, Adv. Phys. **50**, 499 (2001).
19. T. R. McGuire and R. I. Potter, IEEE Transactions on Magnetics, **11**, 1018 (1975)
20. R. C. O'Handley, Modern Magnetic Materials (Wiley, New York, 1999).
21. T. Chen and V. Marsocci, J. Appl. Phys. **43**, 1554 (1972).
22. T. G. M. Rijks, S. K. J. Lenczowsku, R. Coehoorn, and W. J. M. de Jonge, Phys. Rev. B **56**, 362 (1997).
23. W. Gil, D. Gorlitz, M. Horisberger, and J. Kotzler, Phys. Rev. B **72**, 134401 (2005).

24. D. Qu, S. Y. Huang, Jun Hu, Ruqian Wu, and C. L. Chien, Phys. Rev. Lett. **110**, 067206 (2013).
25. Y. M. Lu, Y. Choi, C. M. Ortega, X. M. Cheng, J. W. Cai, S. Y. Huang, L. Sun, and C. L. Chien, Phys. Rev. Lett. **110**, 147207 (2013).
26. F. Wilhelm, P. Poulopoulos, A. Scherz, H. Wende, K. Baberschke, M. Angelakeris, N. K. Flevaris, J. Goulon, and A. Rogalev, Phys. Status Solidi A **196**, 33 (2003).
27. F. Wilhelm, P. Poulopoulos, G. Ceballos, H. Wende, K. Baberschke, P. Srivastava, D. Benea, H. Ebert, M. Angelakeris, N. K. Flevaris, D. Niarchos, A. Rogalev, and N. B. Brookes, Phys. Rev. Lett. **85**, 413 (2000).
28. W. J. Antel, Jr., M. M. Schwickert, Tao Lin, W. L. O'Brien, and G. R. Hap, Phys. Rev. B **60**, 12933 (1999).
29. A. Kobs, S. Heße, W. Kreuzpainter, G. Winkler, D. Lott, P. Weinberger, A. Schreyer and H. P. Oepen, Phys. Rev. Lett. **106**, 217207 (2011).
30. H. Ibach and H. Luth, Solid-state physics: an introduction to principles of materials science (Springer, Berlin, 2009).
31. D. A. Papaconstantopoulos, Handbook of Band Sturcture of Elemental Solids (Plenum Press, New York, 1986).

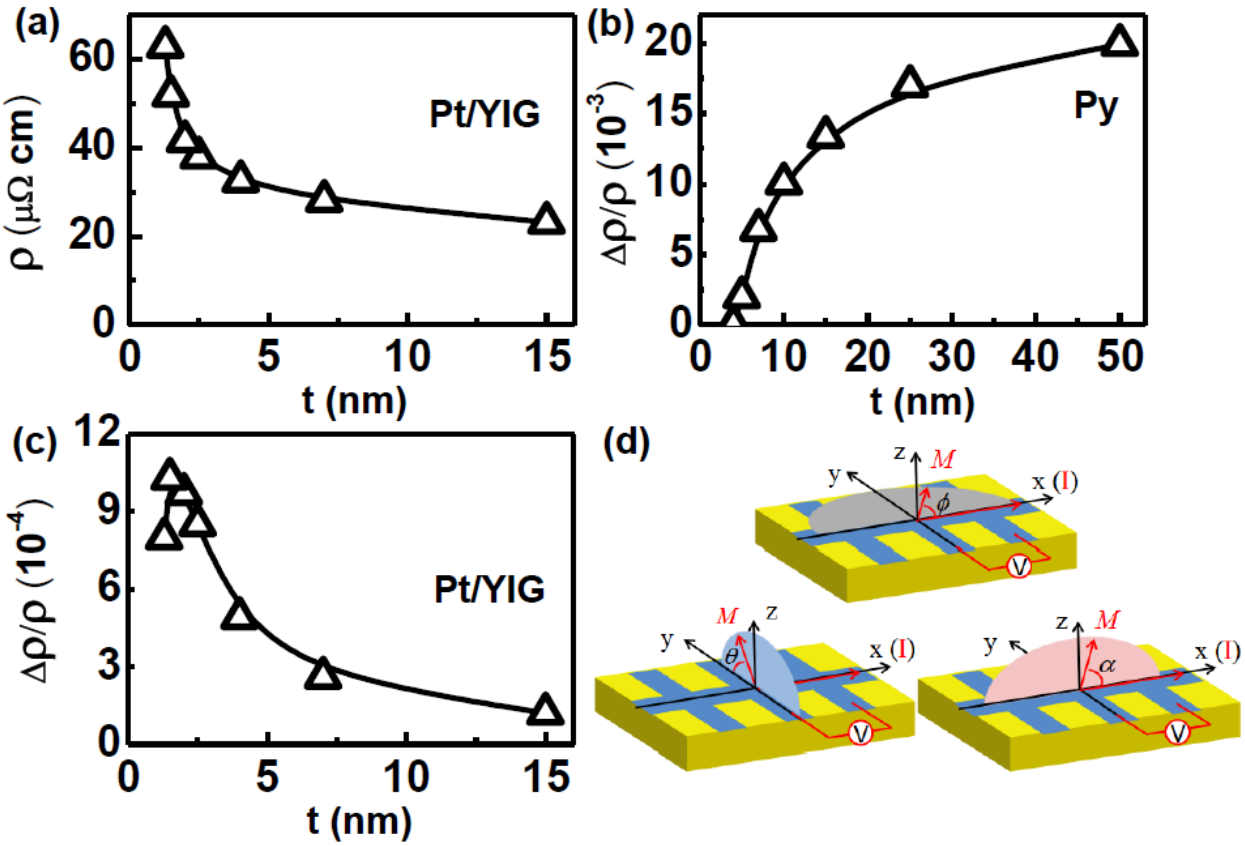

FIG. 1. Thickness (t) dependence of (a) resistivity ρ of Pt films, (b) AMR $\Delta\rho/\rho$ in permalloy (Py) film, and (c) hybrid MR $\Delta\rho/\rho$ in Pt films on YIG at 300 K. (d) MR measurements of Hall-bar thin film in the xy-plane with current along x. The magnetic field can be applied in xy, xz, and yz planes with angle ϕ_{xy}, α_{xz} , and θ_{yz} relative to x, x, and z axes, with the MR results shown in black, red, and blue respectively.

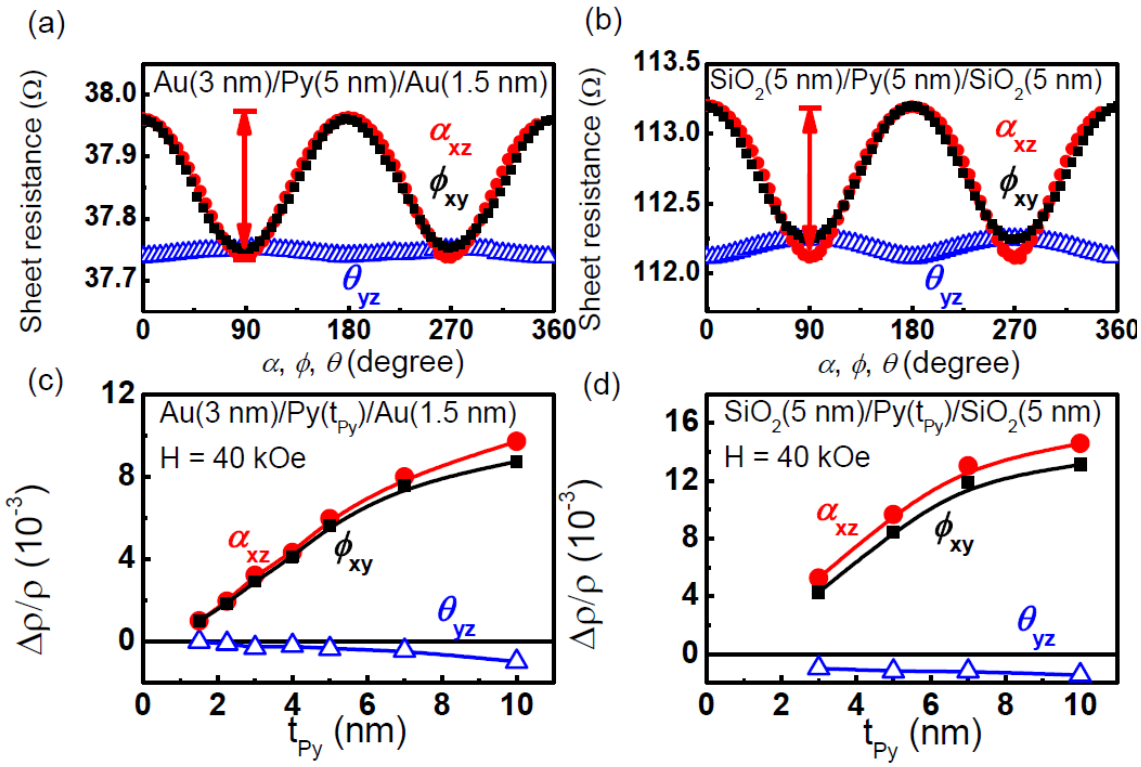

FIG. 2. Angular dependence of MR at 300 K of (a) Au(3 nm)/Py(5 nm)/Au(1.5 nm) and (b) SiO_2(5 nm)/Py(5 nm)/SiO_2(5 nm) in the ϕ_{xy}(black), α_{xz}(red), and θ_{yz} (blue) scan; the AMR dependence on Py thickness t_{Py} of (c) Au/Py(t_{Py})/Au, and (d) SiO_2/Py(t_{Py})/SiO_2.

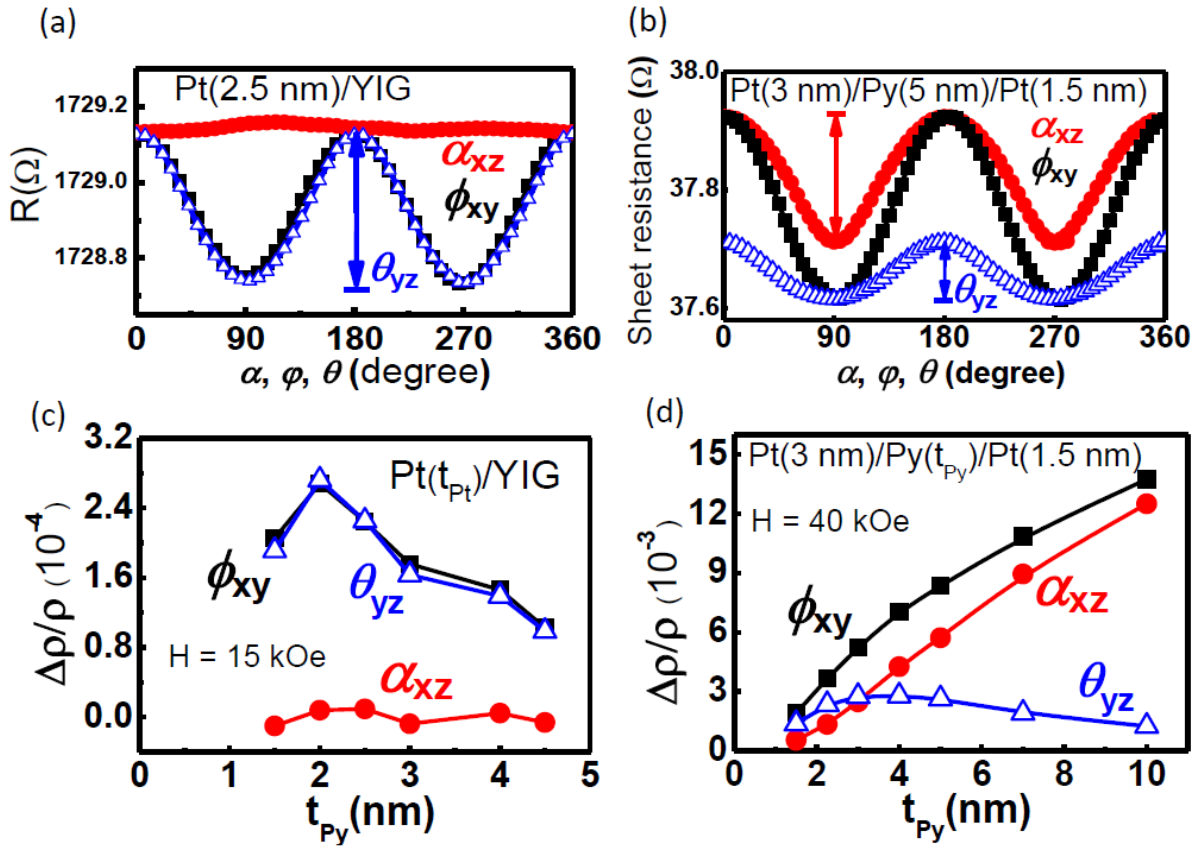

FIG. 3. Angular dependence of MR at 300 K of (a) Pt(2.5 nm)/YIG (polycrystalline), (b) Pt(3 nm)/Py(5 nm)/Pt(1.5 nm) at 300 K in the ϕ_{xy} (black), α_{xz} (red), and θ_{yz} (blue) scan; dependence of $\Delta\rho/\rho$ on thickness t of (c) Pt(t_{Pt})/YIG, and (d) Pt/Py(t_{Py})/Pt.

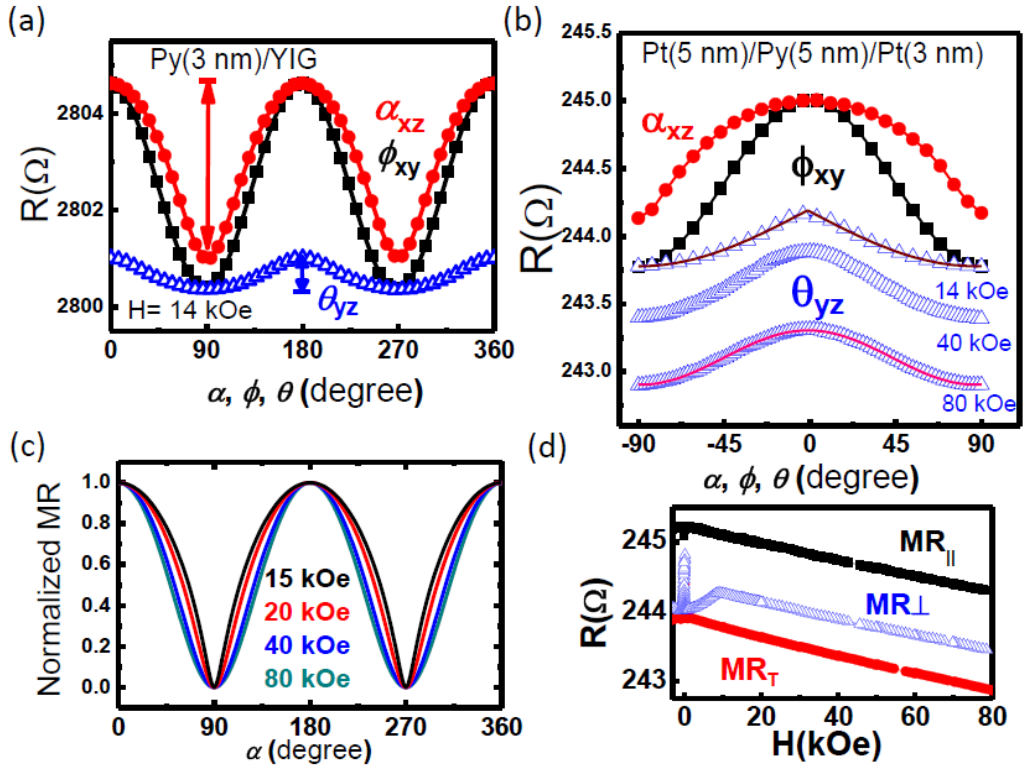

FIG. 4. Angular dependence of MR at 300 K at 14 kOe of (a) Py(4 nm)/YIG, (b) Pt(5 nm)/Py(5 nm)/Pt(3 nm) in the ϕ_{xy}(black) α_{xz}(red), and θ_{yz} (blue) scan; also shown in (b) is field dependence of MR in the θ_{yz} (blue) scan at 40 kOe and 80 kOe, (c) calculated α_{xz}-scan at 15, 20, 40, and 80 kOe, as the angular dependence changes from $|\cos\alpha|$ at low fields to $\cos^2\alpha$ at high fields, (d) field dependence of the three resistivities $\rho_{||}$, ρ_{T} and $\rho_{\perp}$with $\boldsymbol{H}$ along *x, y,* and *z* directions respectively.